The Astrophysical Journal Letters, 908:L38 (12pp), 2021 February 20 https://doi.org/10.3847/2041-8213/abdfcd

Dynamical Formation of the GW190814 Merger

Manuel Arca Sedda
Astronomisches Rechen-Institut, Zentrum für Astronomie der Universität Heidelberg, Mönchhofstr. 12-14, D-69120 Heidelberg, Germany; m.arcasedda@gmail.com
Received 2020 October 16; revised 2021 January 18; accepted 2021 January 26; published 2021 February 22

Abstract

We investigate the possible dynamical origin of GW190814, a gravitational wave (GW) source discovered by the LIGO-Virgo-Kagra collaboration (LVC) associated with a merger between a stellar black hole (BH) with mass $23.2\,M_{\odot}$ and a compact object, either a BH or a neutron star (NS), with mass $2.59\,M_{\odot}$. Using a database of 240,000 N-body simulations modeling the formation of NS–BH mergers via dynamical encounters in dense clusters, we find that systems like GW190814 are likely to form in young, metal-rich clusters. Our model suggests that a little excess (∼2%–4%) of objects with masses in the range of 2.3–3 $M_{\odot}$ in the compact remnants' mass spectrum leads to a detection rate for dynamically formed "GW190814 -like" mergers of $\Gamma_{\rm GW190814} \simeq 1$–$6\,{\rm yr}^{-1}\,{\rm Gpc}^{-3}$, i.e., within the observational constraints set by the GW190814 discovery, $\Gamma_{\rm LVC} \sim 1$–$23\,{\rm yr}^{-1}\,{\rm Gpc}^{-3}$. Additionally, our model suggests that ∼1.8%–4.8% of dynamical NS–BH mergers are compatible with GW190426_152155, the only confirmed NS–BH merger detected by the LVC. We show that the relative amount of light and heavy NS–BH mergers can provide clues about the environments in which they developed.

Unified Astronomy Thesaurus concepts: Astrophysical black holes (98); Stellar astronomy (1583); Gravitational waves (678); Neutron stars (1108); Compact objects (288); Compact radiation sources (289)

1. Introduction

The LIGO-Virgo collaboration (LVC) recently detected GW190814, a merger between a black hole (BH) with mass $M_{\rm BH} = 23.2^{+1.1}_{-1.0}\,M_{\odot}$ and a *mysterious* compact object with mass $M_{\rm CO} = 2.59^{+0.08}_{-0.09}\,M_{\odot}$ (The LIGO Scientific Collaboration et al. 2020). The properties of GW190814 challenge our understanding of compact binaries: (i) the secondary mass falls in the "lower mass gap," a range of masses (2.5–5 $M_{\odot}$) characterized by the observational absence of stellar remnants (Bailyn et al. 1998; Özel et al. 2012); (ii) the mass ratio is small, $q = 0.112^{+0.008}_{-0.008}$; and (iii) the inferred merger rate is fairly large, $\Gamma_{\rm LVC} = 7^{+16}_{-6}\,{\rm yr}^{-1}\,{\rm Gpc}^{-3}$. The unusual mass of the GW190814 secondary suggests that this merger involved either the heaviest neutron star (NS) or the lightest BH known in a compact binary system. Although the BH hypothesis seems to be the favored one (The LIGO Scientific Collaboration et al. 2020), the existence of NSs with masses up to $3\,M_{\odot}$ (e.g., Freire et al. 2008; Tsokaros et al. 2020) or, in general, the absence of a lower mass gap (e.g., Wyrzykowski & Mandel 2020; Zevin et al. 2020) cannot be completely ruled out. Whether the secondary is an NS or a BH, matching all GW190814 features—low-mass companion, low mass ratio, and large merger rate—poses a challenge to astrophysical theories. Population synthesis models for isolated binaries predict mass ratios $q > 0.2$ (Dominik et al. 2012; Marchant et al. 2017; Giacobbo & Mapelli 2018; Spera et al. 2019), unless special prescriptions are adopted (Eldridge et al. 2017; Giacobbo & Mapelli 2018). Formation in active galactic nuclei (AGNs) could be a promising channel, although mergers developing in such extreme environments might have larger BH masses, $M_{\rm BH} \sim 50\,M_{\odot}$ (Yang et al. 2019), but comparable mass ratios, i.e., $q = 0.07 - 0.2$ (Yang et al. 2019; McKernan et al. 2020), in relation to GW190814. Nonetheless, ∼4% of AGN-assisted mergers can have one of the binary components in the lower mass gap (Yang et al. 2020). Other explanations include that the accretion of material expelled during the NS formation remained bound to the binary owing to the large mass of the primary (Safarzadeh & Loeb 2020), through a hierarchical merger involving two NSs and a BH (Lu et al. 2021), or, in general, in hierarchical triples assembled either in the field or in dense clusters (e.g., Liu & Lai 2021). Alternatively, GW190814-like systems may hint at a supernova (SN) mechanism acting on longer timescales than previously thought, thus enabling the proto-compact remnant to accrete enough mass before undergoing explosion (Zevin et al. 2020). However, even in such a case the formation of mergers with a secondary mass and mass ratio compatible with GW190814 is almost impossible in the isolated binary scenario, regardless of the SN explosion mechanism assumed (Zevin et al. 2020). Another potential formation channel for GW190814 is via dynamical encounters in a star cluster. The dynamical formation of massive binaries (e.g., BH–BH) is efficient in globular clusters (GCs), where compact remnants undergo dozens of interactions before either merging inside the cluster or getting ejected and merging afterward (Rodriguez et al. 2016, 2018; Askar et al. 2017). However, binary BHs in GCs tend to have high mass ratios ($q > 0.5$; Rodriguez et al. 2016), while the formation of NS–BH binaries is suppressed owing to BHs that quench mass segregation of lighter objects. Therefore, the inferred NS–BH merger rate for GCs in the local universe is rather low, $\Gamma_{\rm NSBH} = 10^{-2}$–$10^{-1}$ (Clausen et al. 2013; Arca Sedda 2020; Ye et al. 2020). Young and open clusters (YCs) might be suitable formation sites for NS–BH mergers (Ziosi et al. 2014; Rastello et al. 2020). The large number of YCs expected to lurk in galaxies (up to 10^5 in the Milky Way (MW); e.g., Piskunov et al. 2006) can boost the overall NS–BH merger rate, especially if they contain a high fraction of primordial binaries (Rastello et al. 2020). In a recent work, we explored the NS–BH dynamical formation channel through a suite of 240,000 N-body simulations (Arca Sedda 2020) tailored to reproduce scatterings in star clusters with velocity dispersion $\sigma = 5$–$100\,{\rm km\,s}^{-1}$, thus covering the range from YCs to nuclear clusters (NCs). We predict that some NS–BH mergers display distinctive features, namely, a chirp mass $>4\ M_{\odot}$, a BH heavier than $M_{\rm BH} > 10\,M_{\odot}$, and the absence of an electromagnetic (EM) counterpart even if the BH is highly spinning. In this letter, we

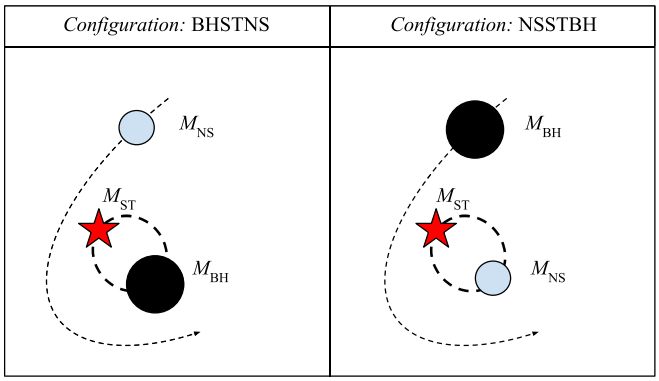

Figure 1. Schematization of the dynamical encounter driving the formation of an NS–BH binary in a dense stellar environment. We assume that either a roaming NS scatters over a BH-star (ST) binary (left panel, configuration BHSTNS) or vice versa (right panel, NSSTBH).

exploit this database to quantify the likelihood for dynamically formed GW190814-like sources.

2. Dynamical NS–BH Merger Rates and the Formation of GW190814-like Sources

Our simulations (Arca Sedda 2020) model binary–single hyperbolic encounters involving two compact objects and a *normal* star, using `ARGdf` (Arca-Sedda & Capuzzo-Dolcetta 2019), an improved version of the `ARCHAIN` N-body code that implements post-Newtonian formalism up to order 2.5 (Mikkola & Merritt 2008) and enables a high-accuracy treatment for close encounters (Mikkola & Tanikawa 1999). We adopt a mass function for compact objects such that all remnants with a final mass $<3\ M_\odot$ are labeled as NSs, while the remaining are labeled as BHs. The database, containing over 240,000 simulations, is dissected into two configurations (see Figure 1): either the binary contains a BH and a star (ST) and the third object is an NS (configuration BHSTNS), or vice versa (NSSTBH). Details about the initial conditions and the mass distribution of the objects involved in the scattering are discussed in Appendices A and B.

We identify $N_{\rm GW}=1193$ mergers, i.e., $P_{\rm NS-BH}\simeq 0.5\%$ of the whole sample. To characterize how $N_{\rm GW}$ varies across different values of the velocity dispersion (σ), we define an *individual merger rate* ($\Gamma_{\rm ind}$), namely, the number of mergers per unit time per cluster, as

$$\Gamma_{\rm ind}=p_{\rm GW}N_{\rm bin}dR/dt, \tag{1}$$

i.e., as the product between the fraction of NS–BH mergers ($p_{\rm GW}$) that is measured directly from our simulations, the average number of binaries containing either an NS or a BH that at a given time coexist in the cluster ($N_{\rm bin}$), and the rate of binary–single interactions that lead to the formation of an NS–BH binary (dR/dt). We find that there is a tight relation between $\Gamma_{\rm ind}$ and σ, well described by a power law

$$\Gamma_{\rm ind}\simeq kN_{\rm bin}\left(\frac{\sigma}{\sigma_c}\right)^{\delta}. \tag{2}$$

In the equation above, $\sigma_c=5\,{\rm km\,s^{-1}}$, and k and δ, whose values are summarized in Table 1, are best-fit parameters calculated through a linear regression fit applied to the database of simulated mergers. The functional form above is likely the result of the relation between the parameters involved in

Table 1
Best-fitting Parameters for Clusters' Individual Merger Rate

Configuration	Z	k ($\rm Gyr^{-1}$)	δ
BHSTNS	0.0002	$(5.2\pm0.9)\times10^{-2}$	0.99 ± 0.01
	0.02	$(3.6\pm0.2)\times10^{-2}$	0.98 ± 0.03
NSSTBH	0.0002	$(1.0\pm0.2)\times10^{-3}$	0.78 ± 0.12
	0.02	$(4.0\pm0.6)\times10^{-4}$	0.89 ± 0.08

Note. Column (1): scattering configuration. Column (2): metallicity. Columns (3)–(4): parameters of the fitting function for the individual merger rate in Equation (2).

Equation (1) and the cluster velocity dispersion. As discussed in Appendix A, the $N_{\rm bin}$ parameter is highly uncertain, as it depends on the mass of the cluster, the retention fraction of both NSs and BHs, and the cluster relaxation time in a nontrivial way. To constrain this quantity, we resort to the suite of GC Monte Carlo models named the MOCCA Survey Database I (Askar et al. 2017). In MOCCA we find on average $N_{\rm bin}\sim1$ for cluster mass $M<10^5\,M_\odot$ and $N_{\rm bin}=2$–4 for heavier clusters. Note that the cluster mass M and half-mass radius r_h are linked to σ via (Arca Sedda 2020)

$${\rm Log}(GM/r_h)=(1.14\pm0.03)+2{\rm Log}\,\sigma; \tag{3}$$

thus, we can uniquely infer the individual merger rate for a cluster with given mass and half-mass radius through its velocity dispersion. Table 2 lists $\Gamma_{\rm ind}$ estimates assuming typical values for σ in YCs, GCs, and NCs. At a redshift $z\lesssim1$, the merger rate associated with a given cluster population can be roughly calculated as (Arca Sedda 2020; Ye et al. 2020)

$$\Gamma_{\rm NS-BH}=\Gamma_{\rm ind}\rho_{\rm MWEG}N_c, \tag{4}$$

where $\Gamma_{\rm ind}$ is calculated through Equation (2), $\rho_{\rm MWEG}=0.0116\,{\rm Mpc^{-3}}$ is the local density of MW-equivalent galaxies (Abadie et al. 2010), and N_c is the total number of clusters in the galaxy. A typical NC has $\Gamma_{\rm NC}<0.5\,{\rm Gyr^{-1}}$, i.e., 1–3 orders of magnitude larger than other cluster types. However, the contribution of NCs to the population of NS–BH binaries is likely rather low, as they are outnumbered by GCs (around 200 in the MW; Harris 2010) and YCs (up to 10^5; Piskunov et al. 2006). Assuming around 200 GCs and 1 NC for all MW-like galaxies in the local universe implies a merger rate $\Gamma_{\rm GC}=(0.002\text{–}0.1)\times N_{\rm bin}\,{\rm yr^{-1}\,Gpc^{-3}}$ and $\Gamma_{\rm NC}=(3\times10^{-5}\text{–}6\times10^{-3})\times N_{\rm bin}\,{\rm yr^{-1}Gpc^{-3}}$. To explain the LVC inferred rate, the number of binaries with a compact object lurking in typical GCs and NCs should thus be $N_{\rm bin}\sim10^4$–10^5. However, $N_{\rm bin}$ is more likely to be $\lesssim10$ in GCs (e.g., Morscher et al. 2015; Kremer et al. 2020; see also Appendix A) and $\sim10^2$–10^3 in NCs (e.g., Arca Sedda et al. 2020), thus suggesting that these environments are unlikely to be the main contributor to the population of NS–BH mergers. Extending our calculations to YCs, instead, yields

$$\Gamma_{\rm YC}=\left(\frac{\rho_{\rm MWEG}}{0.0116\ {\rm Mpc^{-3}}}\right)\left(\frac{N_c}{10^5}\right)N_{\rm bin}\times\begin{cases}0.04\text{–}3.7\ {\rm yr^{-1}\,Gpc^{-3}}, & \sigma=0.3\ {\rm km\ s^{-1}},\\ 0.1\text{–}12.3\ {\rm yr^{-1}\,Gpc^{-3}}, & \sigma=1.0\ {\rm km\ s^{-1}},\\ 0.3\text{–}36.6\ {\rm yr^{-1}\,Gpc^{-3}}, & \sigma=3.0\ {\rm km\ s^{-1}},\end{cases} \tag{5}$$

Table 2
Individual Merger Rate for Different Cluster Types

Cluster Type	M ($M_\odot$)	r_h (pc)	σ (km s^{-1})	$N_{\rm bin}$	$\Gamma_{\rm ind}$ (Gyr^{-1}) NSSTBH Z = 0.0002	NSSTBH Z = 0.02	BHSSTNS Z = 0.0002	BHSSTNS Z = 0.02
YCs	3×10^2	1	0.3 (1)	1	1.17×10^{-4}	3.25×10^{-5}	3.22×10^{-3}	2.24×10^{-3}
YCs	3×10^3	1	1.0 (1)	1	2.99×10^{-4}	9.57×10^{-5}	1.06×10^{-2}	7.37×10^{-3}
YCs	3×10^4	1	3.0 (1)	1	7.06×10^{-4}	2.56×10^{-4}	3.15×10^{-2}	2.18×10^{-2}
GCs	10^5	3	5.5 (2)	1	1.13×10^{-3}	4.41×10^{-4}	5.75×10^{-2}	3.96×10^{-2}
NCs	8×10^6	3	50 (3)	1	6.34×10^{-3}	3.19×10^{-3}	5.13×10^{-1}	3.50×10^{-1}

Note. Columns (1)–(4): cluster type, mass, half-mass radius, and typical velocity dispersion. Column (5): average number of binaries containing an NS or a BH. Columns (6)–(7): individual merger rate for NSSTBH configuration and different metallicities. Columns (8)–(9): individual merger rate for BHSTNS configuration and different metallicities.
References. (1) Piskunov et al. 2007; Soubiran et al. 2018; Jackson et al. 2020; (2) Harris 2010; (3) Feldmeier et al. 2014.

with lower limits corresponding to $Z=0.02$ and the NSSTBH configuration. According to Equation (3), the σ values adopted above correspond to a cluster mass $M_{\rm YC}=(280\text{–}3166\text{–}28{,}000)\,M_\odot$ assuming $r_h=1$ pc. Note that such an optimistic rate is obtained assuming that all MW-like galaxies in the local universe have a number of YCs $\sim10^5$, each of which contains at least $N_{\rm bin}=1$ binary that undergoes the type of scattering explored here.

This rate falls within the LVC measurements (The LIGO Scientific Collaboration et al. 2020) and is in remarkably good agreement with simulations of compact YCs (Rastello et al. 2020). Assuming instead similar number densities for YCs and GCs, $\rho_{\rm GC}=2.31$ Mpc^{-3}, leads to $\Gamma_{\rm YC}=(1.5\times10^{-4}\text{–}0.06)$ yr^{-1} Gpc^{-3}, in agreement with recent results from Fragione & Banerjee (2020; for more details see Appendix E). The agreement between our models and fully consistent N-body simulations, in spite of the different assumptions adopted, suggests that the dynamical formation of NS–BH binaries is driven mostly by stellar dynamics and is less affected by stellar evolution and post-Newtonian corrections. Our simplified approach enables us to produce a catalog of $\sim10^3$ NS–BH mergers, which can be used to constrain their overall properties and to access the NCs' mass range, for which full direct simulations are prohibitive.

3. Dynamical Formation of GW190814 and GW190426_152155

Among all our models, we find 11 mergers with a BH with mass $20<M_{\rm BH}/M_\odot<25$ and an NS with mass $M_{\rm NS}>2\,M_\odot$. One interesting example is BHSTNS15ZH-S5561 (configuration BHSTNS, $\sigma=15$ km s^{-1}, metallicity $Z=0.02$), which has $M_{\rm BH}=23.1\,M_\odot$ and $M_{\rm NS}=2.77\,M_\odot$, i.e., within $\sim$0.4% and $\sim$7% from the GW190814 measured values. As shown in Figure 2, after formation, BHSTNS15ZH-S5561 has a semimajor axis $a=0.6$ au and eccentricity $e=0.97$, merging within $t_{\rm GW}=1.3$ Gyr. Note that the large NS mass is due to the adopted mass spectrum for compact remnants, which enable the formation of NSs with a maximum mass of $\sim3\ M_\odot$ at solar metallicity (see Appendix B).

To identify other NS–BH mergers similar to GW190814, we use the BH mass $M_{\rm BH}$ and the mass ratio q. Figure 3 compares these quantities for GW190814, our dynamical mergers, and isolated mergers (adapted from Giacobbo & Mapelli 2018) for metal-poor ($Z=0.0002$) and metal-rich ($Z=0.02$) stellar progenitors. It must be noted that Giacobbo & Mapelli (2018) adopted a *rapid* SN explosion scheme (see Fryer et al. 2012), whereas our model is based on a *delayed* SN scheme for the calculation of compact remnants' masses. Nonetheless, updated models of isolated binary evolution accounting for both rapid and delayed SN, which have shown a broad agreement with Giacobbo & Mapelli (2018) models, suggest that the amount of mergers with properties similar to GW190814 is limited to <0.1%–1%, regardless of the SN mechanism considered (Zevin et al. 2020).

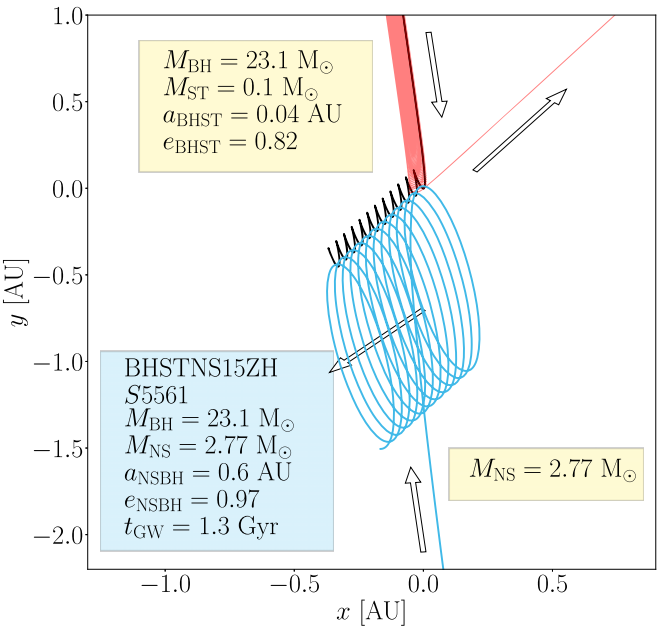

Figure 2. Formation of a GW190814 prototype in one of our models ($Z=0.02$, $\sigma=15$ km s^{-1}). During the scattering, the NS swaps with the star (ST), which is ejected away, leading to the formation of a highly eccentric binary with merging time $t_{\rm GW}\lesssim1.3$ Gyr.

To identify systems similar to GW190814 in our database, we shortlist all mergers having a mass and mass ratio within 30% of the measured values for GW190814. We find a probability $P_{\rm LVC}=4.1\%\text{–}5.9\%$ of finding GW190814-like mergers in metal-poor configurations BHSTNS and NSSTBH, respectively, and $P_{\rm LVC}=8.2\%\text{–}11.3\%$ for solar-metallicity models. From Equation (5) and Table 2 we can thus derive a rate for mergers

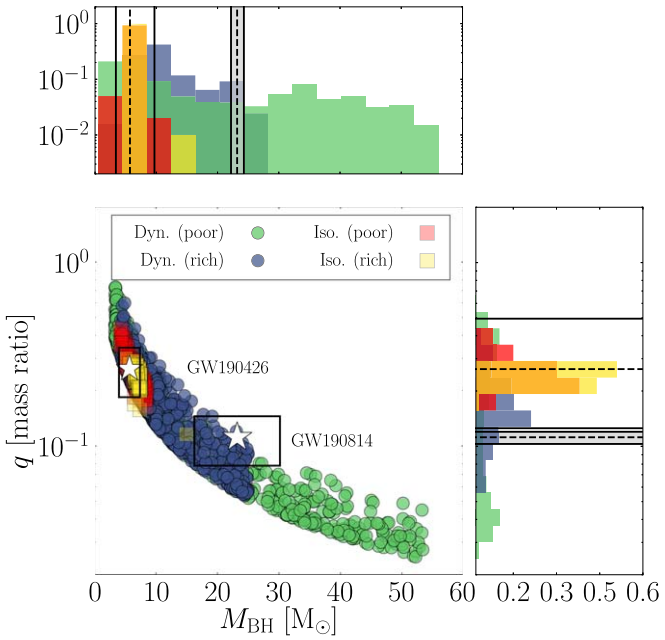

Figure 3. Mass ratio q vs. BH mass $M_{\rm BH}$ for NS–BH mergers in our metal-poor (green circles) and metal-rich (purple circles) models, compared to the measured values for GW190814 and GW190426_152155 (white stars). We include the combined distribution for metal-poor (red squares) and metal-rich (yellow squares) binaries derived from Giacobbo & Mapelli (2018) (model *CC*15α5). The black boxes enclosing GW190814 and GW190426_152155 represent regions deviating <30% from the observed $M_{\rm BH}$ and q. In the side histograms, the dotted lines identify the measured mass and mass ratio for both GW sources, while the shaded (empty) areas encompass the measured 90% credible level for GW190814 (GW190426_152155).

similar to GW190814 in YCs as

$$\Gamma_{\rm LVC} = P_{\rm LVC}\Gamma_{\rm YC} = \begin{cases} (0.01\text{–}2.1) N_{\rm bin}\ {\rm yr}^{-1}\,{\rm Gpc}^{-3} & Z/{\rm Z}_\odot = 0.01, \\ (0.009\text{–}2.9) N_{\rm bin}\ {\rm yr}^{-1}\,{\rm Gpc}^{-3} & Z/{\rm Z}_\odot = 1, \end{cases} \quad (6)$$

with the lower (upper) limits corresponding to the case $\sigma = 1$ (3) km s^{-1}, i.e., the typical value of velocity dispersion for MW young and open clusters (Soubiran et al. 2018; Kuhn et al. 2019; Jackson et al. 2020), and to configuration NSSTBH (BHSTNS).

Using the same procedure, we also search for mergers similar to GW190426_152155, an NS–BH merger detected during the O3 LVC observation run, characterized by $M_{\rm BH} = 5.7^{+4.0}_{-2.3}\,M_\odot$ and $M_{\rm NS} = 1.5^{+0.8}_{-0.5}\,M_\odot$. We find mergers with primary mass and mass ratio within 30% of the measured values for GW190426_152155 in 15% of our models regardless of the progenitor metallicity, thus indicating that dynamical mergers can produce a substantial fraction of systems with a relatively low mass. Note that the interval of $M_{\rm BH}$ and q values assumed in this case falls well within the observed 90% credible interval level.

The analysis above does not account for potential observation biases that can affect GW detectors. For instance, the volume within which LIGO can detect a given class of sources depends on several parameters, like the source mass and mass ratio, the distance, the sky location, or the mutual inclination of the spins. For binaries with a total mass $M_1 + M_2 = (10\text{–}100)\,M_\odot$, Fishbach & Holz (2017) showed that this volume scales with the primary mass following a power law $VT \propto M_1^{2.2}$ and decreases with decreasing mass ratio q. Using Figure 1 in Fishbach & Holz (2017), we extract VT and q at a fixed primary mass value $M_1 = (10,\ 20,\ 25,\ 30,\ 50)\,M_\odot$, finding that such a relation is well described by a power law $VT \propto q^\beta$, with $\beta \sim 0.4$–0.6. In the following, we adopt a slope $\beta = 0.5$, which is the value associated with a primary mass $M_1 \sim 20\,M_\odot$. As we show in Appendix D, setting $q = 0.4$ or $q = 0.6$, i.e., the values typical of systems with a primary $M_1 < 35\,M_\odot$, leads our estimated merger rate to vary by less than 10%. To mimic the selection effect connected with the binary primary and mass ratio, we augment our population of NS–BH mergers to 10,000 by sampling them from the combined $M_{\rm BH}$–$M_{\rm NS}$ distribution, and from the augmented sample we extract 1000 NS–BH mergers, weighing the probability of selecting a given mass and mass ratio with the selection functions $f_M = k_{\rm BH} M_{\rm BH}^{2.2}$ (with $k_{\rm BH}$ a normalization constant) and $f_q = k_q q^{0.5}$ (see also Arca Sedda & Benacquista 2019; Arca Sedda et al. 2020). The resulting *volume-weighted* mass distribution for BHs and NSs and the $M_{\rm BH}$–q plane are shown in Figure 4. The percentage of mergers falling inside the limiting values adopted for GW190814 remains limited to $P_{\rm LVC} = 4.3\% \pm 0.4\%$ for metal-poor clusters, owing to the fact that heavier BHs have a larger probability of being selected. For metal-rich environments and the BHSTNS configuration, instead, this probability increases to $P_{\rm LVC} = 22\% \pm 2\%$, leading to an optimistic "volume-weighted" merger rate for GW190814-like mergers in YCs of

$$\Gamma_{\rm GW190814,V} = \left(\frac{\rho_{\rm MWEG}}{0.0116\ {\rm Mpc}^{-3}}\right)\left(\frac{N_c}{10^5}\right) N_{\rm bin} \times \begin{cases} (0.008\text{–}0.6)\ {\rm yr}^{-1}\,{\rm Gpc}^{-3} & \sigma = 0.3\ {\rm km\ s}^{-1} \\ (0.023\text{–}2.0)\ {\rm yr}^{-1}\,{\rm Gpc}^{-3} & \sigma = 1.0\ {\rm km\ s}^{-1} \\ (0.062\text{–}5.8)\ {\rm yr}^{-1}\,{\rm Gpc}^{-3} & \sigma = 3.0\ {\rm km\ s}^{-1} \end{cases} \quad (7)$$

at redshift $z < 1$ and adopting $\rho_{\rm MWEG} = 0.0116\,{\rm Mpc}^{-3}$, $N_c = 10^5$, and $N_{\rm bin} = 1$ as scaling values. The lower (upper) limit corresponds to configuration NSSTBH (BHSTNS). The same calculation for metal-poor clusters yields a maximum value of 0.005–1.7 yr^{-1} Gpc^{-3}, thus suggesting that a population of metal-rich YCs with $\sigma = 1$–3 km s^{-1}, i.e., $r_h \sim 0.5$–1.5 pc and $M \sim 10^3$–$10^4\,M_\odot$, represent the most suited class of environments to explain the origin of GW190814. In comparison, the isolated scenario predicts a merger rate of <0.1 yr^{-1} Gpc^{-3}, regardless of the assumptions on the SN mechanism (Zevin et al. 2020).

In the case of GW190426_152155, our procedure leads to $P_{\rm LVC} = 1.8\%$–4.7%, with the lower (upper) limit referring to $Z = 0.02$ (0.0002), thus indicating that the contribution of dynamical mergers to the population of low-mass NS–BH mergers can be nonnegligible.

The merger rates above represent optimistic estimates that rely on the assumption that YCs (1) have around solar metallicity, (2) have all the same velocity dispersion, and (3) are $\sim 10^5$ in MW-like galaxies. The discovery of other mergers similar to GW190814, i.e., with chirp masses $\gtrsim 4\ M_\odot$ and mass ratio <0.1, could help in placing constraints on the processes that regulate the formation and evolution of young clusters in the local universe.

Using the volume-weighted catalog, we calculate the percentage of mergers with a primary mass in the range of [<7, 7–15, ⩾15] $M_\odot$ and a companion mass in the range of

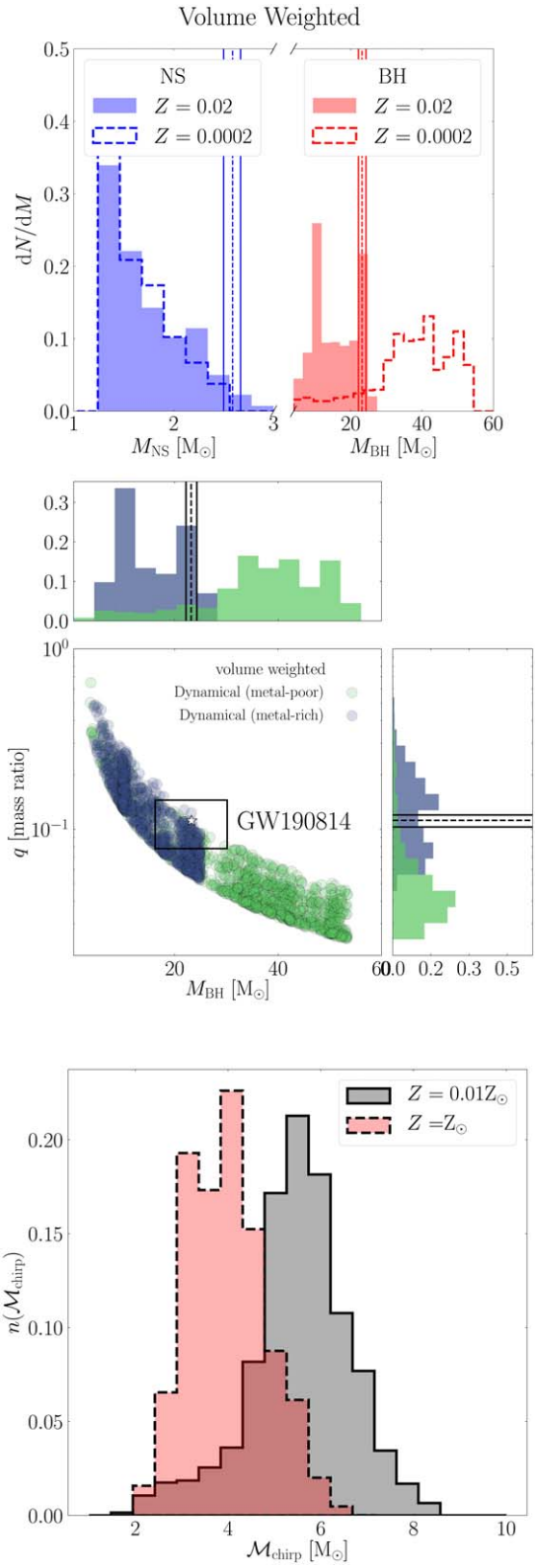

Figure 4. Top: volume-weighted mass spectrum for merging NSs (left, blue) and BHs (right, red) for a metallicity $Z = 0.0002$ (open dashed steps) and $Z = 0.02$ (filled steps). The vertical lines mark the value measured for GW190814 and corresponding uncertainties. Middle: same as in Figure 3, but here the mass ratio and primary mass distribution are weighted with two selection functions to mimic the dependencies affecting the detector accessible volume. Bottom: mergers' chirp mass for metal-rich (filled red steps with dashed edge) and metal-poor (filled gray steps with solid edge) clusters.

[<2, 2–2.5, ⩾2.5] $M_\odot$. As summarized in Table 3, we find that a dominant contribution to NS–BH mergers from metal-rich clusters would result in a 96% probability of detecting a primary heavier than >15 $M_\odot$, whereas for metal-poor clusters this probability is comparable for *light* and *heavy* primary components.

In the extreme case in which NS–BH mergers form dynamically and mostly in metal-rich clusters, the estimate above implies that 9 out of 10 detections of NS–BH mergers would involve a BH with $M_{\rm BH} > 15\,M_\odot$, and 2–3 among them will have a companion with mass >2 $M_\odot$. Comparing these predictions with expectations from other channels and actual detections can help in unraveling the markers of different formation channels in detected sources and shed light on the role of dynamics in determining the assembly of NS–BH mergers.

4. Summary and Conclusions

In this letter we exploited a suite of 240,000 *N*-body simulations of hyperbolic encounters in star clusters to investigate the dynamical formation of NS–BH mergers with properties similar to GW190814 and GW190426_152155. Our main results can be summarized as follows:

1. We find that the NS–BH merger probability depends strongly on the star cluster velocity dispersion, following a power law with slope $\delta \sim 0.6$–1.1. Overall, around 0.5% of our models lead to an NS–BH merger.
2. We derive an individual merger rate, i.e., number of mergers per time unit, for typical NCs (up to ∼0.5 mergers per Gyr), GCs ($<0.06\,{\rm Gyr}^{-1}$), and YCs (<0.01) ${\rm Gyr}^{-1}$.
3. Since YCs outnumber GCs and NCs by a factor of up to 10^5 in typical galaxies, they might be the major contributor to the population of dynamical NS–BH mergers. In the local universe, we infer an NS–BH merger rate for YCs of $\Gamma_{\rm YC} = (0.04$–$36)\,{\rm yr}^{-1}\,{\rm Gpc}^{-3}$.
4. Among all simulations, we identify ∼5%–10% NS–BH mergers with a BH mass and mass ratio compatible with GW190814, and ∼15% with properties similar to GW190426_152155. We exploit our models to derive a "raw" merger rate for dynamically formed GW190814-like sources, i.e., with mass and mass ratio within 30% the observed values, of $\Gamma \sim (0.01$–$2.9)\,{\rm yr}^{-1}\,{\rm Gpc}^{-3}$.
5. To place our models in the context of LVC detections, we assume that the probability of selecting an NS–BH merger in our sample depends on the primary mass ($\propto M_{\rm BH}^{2.2}$) and mass ratio ($\propto q^{0.5}$) to mimic the potential selection effects to which GW detectors might be subjected. This "volume-weighted" sample contains only ∼4.3% ± 0.4% of GW190814-like systems in metal-poor clusters, but this percentage becomes noticeable in metal-rich clusters (∼22% ± 2%).
6. Combining the volume-weighted sample of mergers with the large abundance of YCs in MW-like galaxies, we derive an optimistic rate for GW190814-like mergers of 0.008–5.8 ${\rm yr}^{-1}\,{\rm Gpc}^{-3}$ at low redshift, in the ballpark of LVC predictions and up to 100 times larger than the estimates obtained from isolated binary stellar evolution models.

Table 3
Occurrence of NS–BH Mergers in Different Mass Ranges

Z	$M_{\rm NS}$ ($M_\odot$)			$M_{\rm BH}$ ($M_\odot$)			($M_{\rm BH}$, $M_{\rm NS}$) ($M_\odot$)
	<2	2–2.5	⩾2.5	<7	7–15	⩾15	>7 and >2
0.0002	77.8%	19.5%	2.7%	4.0%	40.9%	55.2%	13.5%
0.02	87.4%	12.3%	0.3%	1.3%	3.3%	95.5%	23.9%

Note. Column (1): metallicity. Columns (2)–(4): probability of having an NS mass within a given mass range. Columns (5)–(7): same as Columns (2)–(4), but for BHs. Column (8): probability of having a merger with a primary mass >7 $M_\odot$ and a companion mass >2 $M_\odot$.

7. Using the same selection procedure, we find ∼1.8%–4.7% of mergers with properties comparable to GW190426_152155, with the lower limit corresponding to metal-poor clusters. This relatively low occurrence disfavors, but does not rule out, a dynamical origin for GW190426_152155.
8. We suggest that the mass spectra of compact remnants in NS–BH merger candidates can be used to identify markers of different formation channels. In the extreme case in which all mergers formed dynamically in metal-rich clusters, we predict that 9 out of 10 mergers should involve a BH with $M_{\rm BH} > 15\,M_\odot$, and at least 2 of them involve a companion with mass >2 $M_\odot$. Comparing these predictions with future detections can shed light on the dynamical channel and provide new insights on the mass spectrum of compact objects in the lower mass gap range.

M.A.S. acknowledges financial support from the Alexander von Humboldt Foundation for the research program "The evolution of black holes from stellar to galactic scales," the Volkswagen Foundation Trilateral Partnership through project No. I/97778 "Dynamical Mechanisms of Accretion in Galactic Nuclei," and the Deutsche Forschungsgemeinschaft (DFG, German Research Foundation)—Project-ID 138713538—SFB 881 "The Milky Way System." M.A.S. is grateful to Martina Donnari for providing useful comments on an earlier version of this manuscript.

Appendix A
Initial Conditions. I. Binary–Single Interaction Rates

The idea at the basis of our approach is that BH-NS binaries form via interaction of a free-roaming single compact object (a BH or NS) and another compact object (an NS or BH) paired with a star. Here we consider "NSs" all compact objects with a mass <3 $M_\odot$ and "BHs" otherwise. Since the two compact objects are heavier than the star, on average this configuration favors the ejection of the least massive component and the formation of a binary with a higher binding energy (Sigurdsson & Phinney 1993). We explore two different configurations: NSSTBH (NS–star binary impacting over a single BH), and BHSTNS (BH–star binary impacting over a single NS), and we vary the stellar metallicity to either $Z = 0.0002$ or $Z = 0.02$ and the cluster velocity dispersion to $\sigma = 5$–15–20–35–50–100 km s^{-1}, thus covering the range of values going from YCs to GCs and NCs.

In such stellar ensembles, the interaction rate between a binary with component mass $M_{1,2}$, semimajor axis a, and eccentricity e and a single object with mass M_3 can be written as

$$dR/dt = \dot{R} = N_{\rm bin} n \sigma \Sigma, \tag{A1}$$

where $N_{\rm bin}$ is the average number of binaries coexisting in the cluster that contain either an NS or a BH, n is the density of scattering stars, σ is the environment velocity dispersion, and Σ is the binary cross section

$$\Sigma = \pi a^2 (1-e)^2 \left[1 + \frac{2G(M_1+M_2+M_3)}{\sigma^2 a (1-e)}\right]. \tag{A2}$$

The density of a population of $N_{\rm CO}$ (either BHs or NSs) with mean mass $\langle M_{\rm CO}\rangle$ inhabiting a cluster with mass M and half-mass radius R_h can be estimated as $n_{\rm CO} \sim N_{\rm CO}/(R^3_{\rm CO})$. For BHs, this quantity can be inferred, for instance, from recent studies on BH retention fraction and consequent formation of a tight BH subsystem (Breen & Heggie 2013; Morscher et al. 2015; Arca Sedda et al. 2018). In this work, we assume that the segregated population of BHs has a density comparable to the overall density of the cluster, $n_{\rm BH} \sim M/(\langle M_{\rm BH}\rangle R_h^3)$, as suggested in Arca Sedda et al. (2018). For NSs instead, we consider the fact that mass segregation is prevented by the presence of BHs in the cluster center and that their total mass is around 0.01 times the cluster mass. Thus, we adopt $n_{\rm NS} = 0.01 n_{\rm GC}$ as an upper limit on the average density of NSs. The number of binaries in the cluster is a crucial parameter. To bracket this quantity, we take advantage of the MOCCA Survey Database I (Askar et al. 2017), a suite of around 2000 Monte Carlo models of star clusters with initial masses in the range $M = 2.4\times10^4$–$7.7\times10^5\,M_\odot$, thus covering the mass range of massive YCs and GCs.

Using the MOCCA models, we calculate the average number of binaries containing a BH (NS) in a cluster at different times (0.5, 1, 3, 6, and 12 Gyr) and in different mass bins, as shown in Figure 5.

The figure highlights a clear, although nontrivial, dependence between $N_{\rm bin}$ and the cluster mass. Clusters lighter than $M < 10^5\,M_\odot$ are characterized by $N_{\rm bin} \sim 1$ for NS in binaries regardless of the cluster mass, while it ranges in between $N_{\rm bin} \sim 1$ and 3 for BHs, especially at earlier times. This is likely due to the fact that low-mass clusters have shorter relaxation times; thus, the formation of binaries containing BHs and their ejection via strong scatterings occur earlier compared to large mass clusters. At values $M > 10^5\,M_\odot$ instead, the number of BHs in binaries varies between $N_{\rm bin} = 1$ and 10, almost regardless of the time, whereas the number of NSs in binaries tends to be smaller, $N_{\rm bin} = 1$–4, especially at earlier times. Given this nontrivial behavior, in our calculations we leave $N_{\rm bin}$ as a scaling value.

We note that this assumption is compatible with results of other models (see, e.g., Morscher et al. 2015), even the most recent one that implements updated stellar evolution for binary and single stars, new prescriptions for SN explosion mechanisms and recoil kicks, and post-Newtonian formalism for compact object interactions (e.g., Kremer et al. 2020), thus

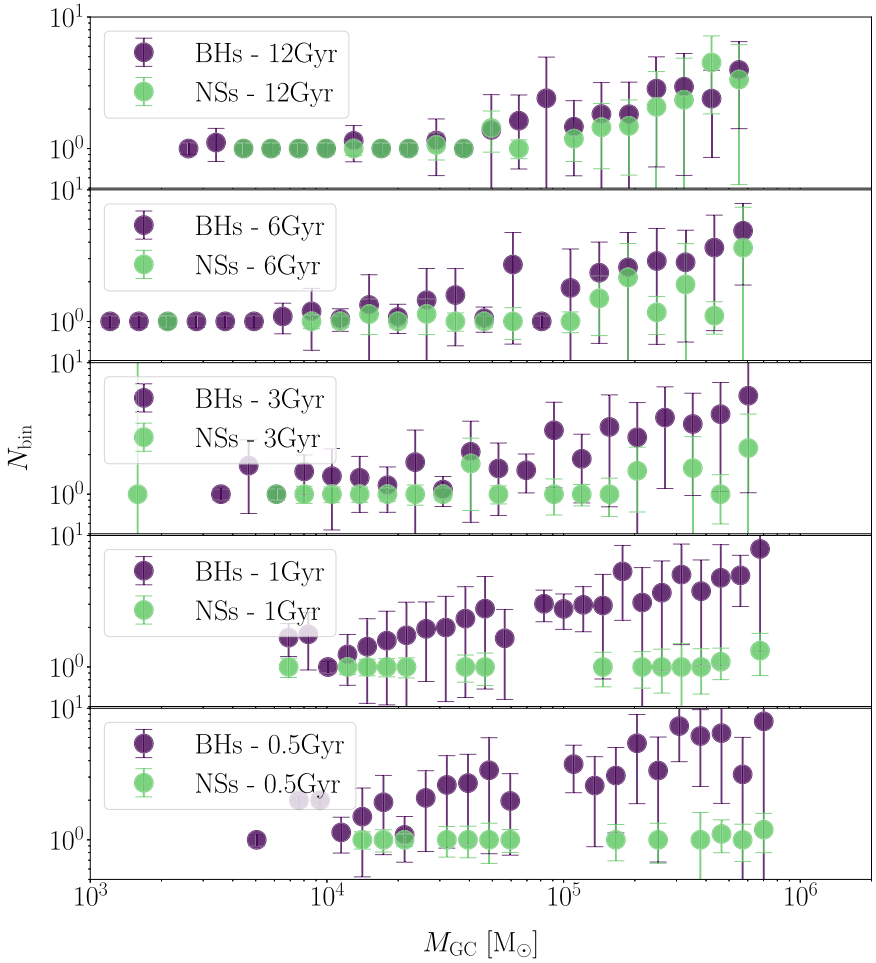

Figure 5. Average number of BHs and NSs in binaries as a function of the cluster mass and for different times; from top to bottom the time considered is 12, 6, 3, 1, and 0.5 Gyr, respectively.

suggesting that the number of binaries left in the cluster at late evolutionary stages is likely the result of dynamics, rather than other mechanisms that, on the other hand, can affect the cluster structure.

Under the set of assumptions above, adopting a cluster velocity dispersion of $\sigma = 5\,{\rm km\,s^{-1}}$, and using the median values of the masses of the binary and third object and the binary semimajor axis and eccentricity, we estimate an interaction rate of $\dot{R} \sim 2$–$4\,{\rm Gyr^{-1}}$ for configuration NSSTBH and $\dot{R} \sim 150$–$400\,{\rm Gyr^{-1}}$ for configuration BHSTNS.

To check the reliability of our calculations, we compare our results with MOCCA models as described in our companion paper (Arca Sedda 2020), finding a range of values fully compatible with our theoretical estimate.

Appendix B
Initial Conditions. II. Mass and Orbital Properties of Binary–Single Scattering Experiments

The binary–single scattering configuration explored in this work is characterized by the masses of the three objects (star, BH, and NS), the orbit of the initial binary, and the orbital properties of the single–binary interaction.

We sample the zero-age main-sequence (ZAMS) mass of the three objects from a Salpeter mass function. At metallicity values $Z = 0.0002$ (0.02), we assume that all stars with a ZAMS mass $M_{\rm minBH} > 20.5$ (18) $M_\odot$ evolve into BHs (Belczynski et al. 2002; Spera & Mapelli 2017), whereas lighter stars with a mass above $M_{\rm minNS} > 8$ (6.5) $M_\odot$ evolve into NSs.

For stars, we select only masses in the range of 0.1–1 $M_\odot$. This choice is motivated by the fact that the timescale associated with the binary–single scatterings modeled here is 10–100 times longer than the half-mass relaxation time of the host cluster (see Appendix C), thus generally longer than the evolutionary time for stars with a mass $m > 2\ M_\odot$, which is $t_{\rm age} = 10\,{\rm Gyr}(m/M_\odot)^{-2.5} \lesssim 1$–$1.5\,{\rm Gyr}$, depending on the metallicity. Stars with a mass $1 < M_{\rm st}/M_\odot < 2$, which constitute 2% of the whole stellar population, evolve on timescales (1.5–9 Gyr) comparable to the cluster relaxation time, depending on the cluster velocity dispersion. For these stars, a proper modeling should also consider the evolutionary stage of the star, a feature that cannot be accounted for in our N-body models. Given the fact that they constitute a small fraction of the stellar population, as stars with a mass $<1\ M_\odot$ constitute over 95.5% of the whole population, and that their stellar evolution timescale is close to (or even longer than) the typical time for the scatterings studied here, we exclude 1–2 $M_\odot$ stars from our models.

For BHs, we adopt the mass spectrum described in Spera & Mapelli (2017, hereafter SM17). In SM17 the authors use the SEVN tool. This tool implements prescriptions for single stellar evolution that include several SN explosion mechanisms and a

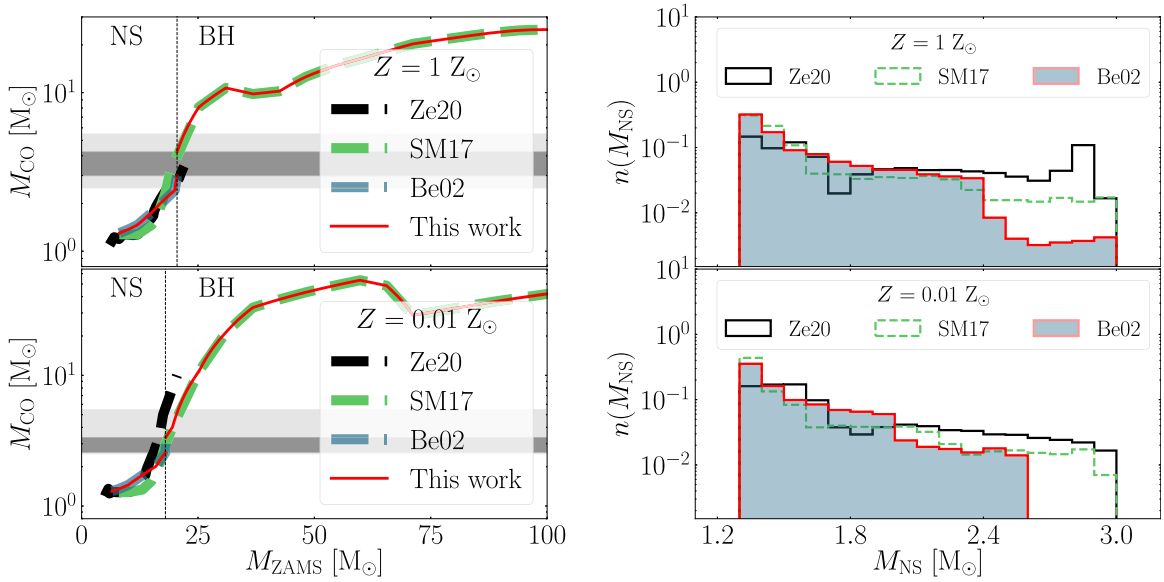

Figure 6. Left panel: final mass for compact objects as a function of the ZAMS mass adopted in this work (straight thin red line) in comparison with Ze20 (dashed thick black line), SM17 (dashed thick light-green line), and Be02 (dashed thick light-blue line) models. The light-gray area encompass the supposed lower mass gap, whereas the dark-gray area labels the mass gap featured in our models. Right panel: NS mass spectrum adopted in this work (thick red line) compared with Ze20 (black steps), SM17 (dashed green steps), and Be02 (filled blue steps).

treatment for pair instability and pulsational pair instability SNe, which naturally lead to a dearth of compact remnants with a mass in the range of 65–120 $M_\odot$ (the so-called upper mass gap). To derive the BH mass from the ZAMS mass, we exploit Tables 1–3 in Spera & Mapelli (2017),[1] according to which the compact remnant mass is calculated adopting the delayed SN explosion mechanism (Fryer et al. 2012).

For NSs, instead, we adopt the single-star stellar evolution model from Belczynski et al. (2002, hereafter Be02) implemented in the BSE package (Hurley et al. 2002). The maximum NS mass in our models reaches ∼2.5 (3) $M_\odot$ for $Z = 0.0002$ (0.02), with a small fraction of NSs (0.03–0.05) at solar metallicities having a mass $M_{NS} > 2.3\,M_\odot$, thus enabling us to explore the lower mass gap region.

The combined use of SM17 prescriptions for BHs and Be02 for NSs leads our simulations to naturally exhibit a narrow lower mass gap in the ranges of 3–4.2 $M_\odot$ at solar metallicity and 2.6–3.1 $M_\odot$ for metal-poor systems. Figure 6 compares the relation between the ZAMS and the remnant masses and the compact remnants' mass spectrum adopted here, in SM17, and in Be02 and the single stellar evolution models described in Ze20. We note that the mass spectrum adopted here is halfway between the case in which a wide lower mass gap does exist and that in which NSs and BHs are linked by a continuous mass spectrum, and we can provide a description of how the delayed SN mechanism, or, more generally, an explosion mechanism that leads to a narrower mass gap, can impact the properties of dynamically formed NS–BH mergers. In fact, our simulations suggest that an excess of 3%–5% of compact remnants with masses in the range of 2.3–3 $M_\odot$ can lead to a dynamical merger rate compatible with LIGO expectations.

We note that the delayed SN model adopted here is only one among many possibilities (e.g., rapid SN mechanism, Fryer et al. 2012; electron-capture SN, Podsiadlowski et al. 2004). Nonetheless, none of the current models in the literature are capable of capturing the complex phases of SN physics, especially in the case of core-collapse SNe, which can be altered significantly by stellar rotation (Mapelli et al. 2020) and require full 3D hydrodynamical simulations to be fully unveiled (e.g., Burrows et al. 2019). From the theoretical point of view, recent single and binary stellar evolution population syntheses suggest that matching the GW190814 features requires that SN explosion proceeds on a timescale longer than typically assumed (e.g., Zevin et al. 2020, hereafter Ze20). Moreover, observations of NSs and BHs detected through their electromagnetic counterparts seem to be inconclusive about the existence of a lower mass gap, suggesting that it might be populated by both massive NSs (Freire et al. 2008) and light BHs (Giesers et al. 2018; Thompson et al. 2019). This is also suggested by recent measurements based on microlensing events detected by the OGLE survey coupled with GAIA DR2 data, which favor a continuous mass spectrum in the 2–5 $M_\odot$ mass range, rather than a lower mass gap (Wyrzykowski & Mandel 2020).

Regarding the orbital properties of the binary and the incoming object, as detailed in our companion paper (Arca Sedda 2020), we assume that the binary–single interaction is hyperbolic and in the regime of strong deflection. For the binary, we adopt as the minimum semimajor axis the maximum between 100 times the star's Roche lobe and 1000 times the innermost stable circular orbit (ISCO) of the compact object in the binary, to avoid the star being disrupted or swallowed before the scattering takes place. The maximum semimajor axis allowed is, instead, calculated as the minimum between the hard-binary separation (Heggie 1975) and the relation suggested by Rodriguez et al. (2016), who have shown that dynamically processed binaries have typical semimajor axis proportional to the binary reduced mass μ and the ratio between the cluster mass and semimajor axis, namely, $a \sim k_d \mu M / R_h$. We adopt $k_d = 10$, which produces a semimajor-axis distribution in full agreement with binary–single scatterings of this kind found in MOCCA simulations with $\sigma = 5\,\mathrm{km\,s^{-1}}$ (see Figure 10 in Arca Sedda 2020).

[1] The SEVN code was not publicly available when this study began.

Appendix C
Criteria for the Identification of Merger Candidates

To identify NS–BH merger candidates, we refine the selection procedure described in Arca Sedda (2020) as follows. We first calculate the GW timescale $t_{\rm GW}$ for all binaries, assuming (Peters 1964)

$$t_{\rm GW} = \frac{5}{256}\frac{c^5 a_f^4 f(e_f)}{G^3 M_1 M_2 (M_1+M_2)} \tag{C3}$$

and

$$f(e) = \frac{(1-e^2)^{7/2}}{1+(73/24)e^2+(37/96)e^4}. \tag{C4}$$

We mark all NS–BH binaries with $t_{\rm GW} < 14$ Gyr as "merger candidates." To determine whether these candidates can undergo merger in a cluster environment, we need to infer the time at which the scattering takes place, i.e., the NS–BH binary formation time t_f, and the timescale over which the binary can get disrupted, e.g., via further strong encounters or secular perturbations.

In a real cluster, the NS–BH binary formation time t_f depends on a number of factors: the mass segregation timescale, the core-collapse process, the formation of binaries and multiples in the cluster core, and the formation or not of a BH subsystem. All these features are not captured by our three-body models, but they are naturally accounted for in the MOCCA models. Therefore, we use a multistepped approach exploiting these high-resolution Monte Carlo models. First, we use the MOCCA database to reconstruct the logarithmic distribution of the ratio between t_f and the half-mass cluster relaxation time calculated at 12 Gyr for all NS–BH binaries formed in MOCCA models,

$$\mathrm{Log}\,\tau \equiv \mathrm{Log}(t_f/t_r), \tag{C5}$$

where the relaxation time is calculated as (Binney & Tremaine 2008)

$$t_r = \frac{0.65\ \mathrm{Gyr}}{\log(\Lambda)}\sqrt{\frac{M_c}{10^5\,M_\odot}}\left(\frac{r_h}{1\ \mathrm{pc}}\right)^{3/2}. \tag{C6}$$

This enables us to provide an estimate of t_f for a given value of the cluster relaxation time, which is directly connected with the cluster velocity dispersion, mass, and half-mass radius (Binney & Tremaine 2008).

The disruption of the NS–BH binary can be driven by either *impulsive* mechanisms, e.g., due to a strong encounter with another compact object, or *diffusive* mechanisms, e.g., due to the effect of the continuous interactions with passing-by stars or the mean field of the cluster.

If the binary is soft, i.e., $G(M_1+M_2)/(2\sigma^2 a) > 1$ (Heggie 1975), we can distinguish between a *catastrophic* regime, i.e., the binary is disrupted in a single interaction, and a *diffusive* regime, i.e., the binary is disrupted owing to the secular effect impinged by interactions with cluster stars. A catastrophic interaction occurs if the impact parameter falls below a maximum value (Binney & Tremaine 2008)

$$b_{\rm max} = 1.5a\left(\frac{GM_p}{(M_1+M_2)\sigma^2 a}\right)^{1/4}; \tag{C7}$$

otherwise, the binary evolution is dominated by the secular, diffusive mechanism.

In the catastrophic regime, the binary disruption occurs over a timescale (Bahcall et al. 1985)

$$t_{\rm cat} = 4.5\ \mathrm{Gyr}\left(\frac{k_{\rm cat}}{0.07}\right)\left(\frac{3000\,M_\odot\ \mathrm{pc}^{-3}}{\rho}\right) \times \left(\frac{M_1+M_2}{20\,M_\odot}\right)^{1/2}\left(\frac{10\ \mathrm{au}}{a}\right)^{3/2}. \tag{C8}$$

In the diffusive regime, the binary can disrupt via high-speed encounters with perturbers of mass M_p, a process characterized by a timescale $t_{\rm ds}$ (Heggie 1975; Binney & Tremaine 2008),

$$t_{\rm ds} \simeq 1.9\ \mathrm{Gyr}\left(\frac{k_d}{0.002}\right)\left(\frac{\sigma}{40\ \mathrm{km\ s^{-1}}}\right)\left(\frac{M_1+M_2}{20\,M_\odot}\right) \times \left(\frac{20\,M_\odot}{M_p}\right)^2\left(\frac{10\ \mathrm{pc}^{-3}}{n_p}\right)\left(\frac{10\ \mathrm{au}}{a}\right), \tag{C9}$$

where k_d is a factor inferred from scattering experiments (Bahcall et al. 1985) and n_p represents the perturbers' number density. However, if these encounters are sufficiently rare the binary can undergo disruption due to the cumulative, secular effect of all the weak interactions with cluster stars. This process takes place over an evaporation time t_e (Binney & Tremaine 2008):

$$t_{\rm ev} \simeq 17.5\ \mathrm{Gyr}\left(\frac{\sigma}{40\ \mathrm{km\ s^{-1}}}\right)\left(\frac{\rho_p}{100\ M_\odot\ \mathrm{pc}^3}\right) \times \left(\frac{a}{10\ \mathrm{au}}\right)\left(\frac{\log\Lambda}{6.5}\right). \tag{C10}$$

If the binary is hard, instead, an interaction with a passing-by star tends, on average, to harden the binary further (Heggie 1975). As the binary hardens, the encounters become rarer but more violent, possibly resulting in the ejection of the binary over a time

$$t_{\rm ej} = \left(\frac{k_{\rm hd}}{100}\right)\left(\frac{t_r}{0.13}\right), \tag{C11}$$

where t_r is the cluster relaxation time and $k_{\rm hd}$ is a parameter derived from scattering experiments (Goodman & Hut 1993; Heggie & Hut 2003).

All the timescales listed above depend on the cluster properties and the average values of scattering parameters. However, our three-body simulations are (a) uniquely defined by the cluster velocity dispersion, which is degenerate in the cluster mass and half-mass radius through Equation (3), and (b) do not take into account the disruption, evaporation, or ejection processes. To partly solve the degeneracy and provide a more reliable description of the possible NS–BH outcomes, we adopt the following treatment to determine whether the NS–BH is likely to survive further stellar encounters and eventually merge.

For each NS–BH merger candidate we create a sample of 100 clusters with the same velocity dispersion but a half-mass radius selected from the observed distribution for GCs (Harris 2010) and NCs (Georgiev & Böker 2014; Georgiev et al. 2016). For each cluster model, we create 100 different

scattering parameters to obtain all the relevant timescales in Equations (C5)–(C11). First, we select the formation time through the following steps:

1. extract the τ value from the distribution reconstructed through MOCCA models;
2. extract the cluster half-mass radius r_h from the observed distribution of Galactic GCs and local NCs;
3. combine r_h and σ (which is fixed for each model) to calculate the cluster mass M_c and the corresponding relaxation time t_r from Equation (C6);

for each ith version of the same NS–BH merger candidate in a different environment, the formation time is thus uniquely defined as $t_{f,i} = \tau_i t_{r,i}$. This sampling is done for each value of the velocity dispersion explored here, i.e., $\sigma = 5,\ 15,\ 20,\ 35,\ 50,$ and $100\,\mathrm{km\,s^{-1}}$.

To characterize the disruption processes, instead, we extract an impact parameter b_i from a linear distribution $2bdb$, as expected from geometrical considerations, limited above by the cluster free mean path and below by 0.1 times the binary semimajor axis, i.e., sufficiently hard to pose a threat to the binary survival.[2] The mass of the perturber is extracted from a power-law mass function with slope $\alpha_{\rm MF} = -2.3$ limited in the range $M_p = 0.08$–$60\,M_\odot$. However, it must be noted that if the cluster core is dominated by heavy remnants, the mass function can be significantly steeper. For instance, if the cluster contains a BH subsystem, Arca Sedda et al. (2018) suggested that half of the mass inside the subsystem is contributed from stars and the remaining in BHs. If we assume that stellar BHs have masses in the range of 5–60 $M_\odot$ and that the overall mass function in the subsystem is described by a power law, it is possible to show that inside the subsystem $\alpha_{\rm MF} \sim -1$. We found that a steeper mass function decreases the number of merger candidates by 12%.

If the binary is soft, we check whether it is in the diffusive ($b_i > b_{\rm max}$) or in the catastrophic regime, calculating the corresponding disruption timescales.

According to this statistical procedure, each NS–BH is characterized by 10,000 potential outcomes. We identify as potential mergers those fulfilling one of the following conditions:

1. $t_{\rm GW} + t_f < t_{\rm cat}$ if the binary is soft and in the catastrophic regime;
2. $t_{\rm GW} + t_f < \min(t_{\rm ds}, t_{\rm ev})$ if the binary is soft and in the diffusive regime;
3. the binary is hard.

If one of the conditions is fulfilled in at least 5% of the interactions modeled for the same NS–BH candidate, we label it as a merger. The number of times the merging binary has been identified as hard ($N_{\rm hd}$) or soft ($N_{\rm sft}$) determines the binary status, which is labeled as "hard" if $N_{\rm hd} > N_{\rm sft}$ or "soft" otherwise. Similarly, we label the merger as in-cluster or ejected depending on the number of times that the binary has been identified as a candidate for ejection before merging or not.

We repeated the same procedure 10 times to verify the impact of randomization on the calculation of the individual merger rate (Equation (2)), and we notice an overall variation of 2%–4% in the values quoted in Table 4.

[2] We verified that decreasing further this limit does not impact the results.

Table 4
NS–BH Mergers in Different Configurations

Configuration	Z ($z_\odot$)	σ ($\mathrm{km\,s^{-1}}$)	$f_{\rm sft}$ (%)	$f_{\rm hd,in}$ (%)	$f_{\rm hd,ej}$ (%)
NSSTBH	0.0002	5	0.0	100.0	0.0
	0.0002	15	0.0	95.2	4.8
	0.0002	20	0.0	90.3	9.7
	0.0002	35	0.0	98.5	1.5
	0.0002	50	1.7	98.3	0.0
	0.0002	100	15.5	84.5	0.0
BHSTNS	0.0002	5	0.0	100.0	0.0
	0.0002	15	0.0	90.9	9.1
	0.0002	20	0.0	95.5	4.6
	0.0002	35	2.3	97.7	0.0
	0.0002	50	7.3	91.0	1.8
	0.0002	100	5.5	94.5	0.0
NSSTBH	0.02	5	0.0	100.0	0.0
	0.02	15	4.0	88.0	8.0
	0.02	20	0.0	88.1	11.9
	0.02	35	0.0	95.1	4.9
	0.02	50	3.0	94.1	3.0
	0.02	100	10.6	88.7	0.7
BHSTNS	0.02	5	0.0	100.0	0.0
	0.02	15	0.0	91.7	8.3
	0.02	20	0.0	94.4	5.6
	0.02	35	0.0	98.5	1.5
	0.02	50	1.0	99.0	0.0
	0.02	100	4.4	95.6	0.0

Note. Column (1): configuration. Column (2): cluster metallicity. Column (3): cluster velocity dispersion. Columns (4)–(6): percentage of mergers from soft binaries, from hard binaries merging inside the cluster, and from hard binaries merging outside the cluster.

In general, we find that the vast majority of NS–BH mergers in our models come from hard binaries (>84%–100%), with the fraction reaching the maximum in correspondence to lower-velocity dispersion clusters. Around 10% of mergers in hard binaries and in clusters with $\sigma = 15$–$35\,\mathrm{km\,s^{-1}}$ are ejected from the parent cluster before the merger takes place.

Appendix D
The Role of the Detector Sensitivity

The detection of a GW source depends intrinsically on several parameters, such as the distance at which the merger took place, the direction of the wave hitting the detector, and the properties of the binary emitting GWs. Recently, Fishbach & Holz (2017) have shown that the volume (VT) accessible to the LIGO detector scales with the mass of the primary through a power law $VT \propto M_1^{\alpha}$, with $\alpha = 2.2$, assuming $10 < M_1/M_\odot < 100$ and at a fixed mass ratio, and increases with increasing mass ratio if the primary mass is kept fixed (see, e.g., their Figure 1). In order to take into account this observational bias in our analysis, we extract the data from Figure 1 of Fishbach & Holz (2017).[3] We associate with the extracted data a conservative error of 10% and reconstruct the dependence between the volume and the mass ratio at fixed primary mass. As shown in Figure 7, we find, for primary masses in the range of 10–50 $M_\odot$, that the volume–mass ratio relation is well represented by a power law $VT \propto q^{\beta}$ with a

[3] We use the data extraction tool https://apps.automeris.io/wpd/.

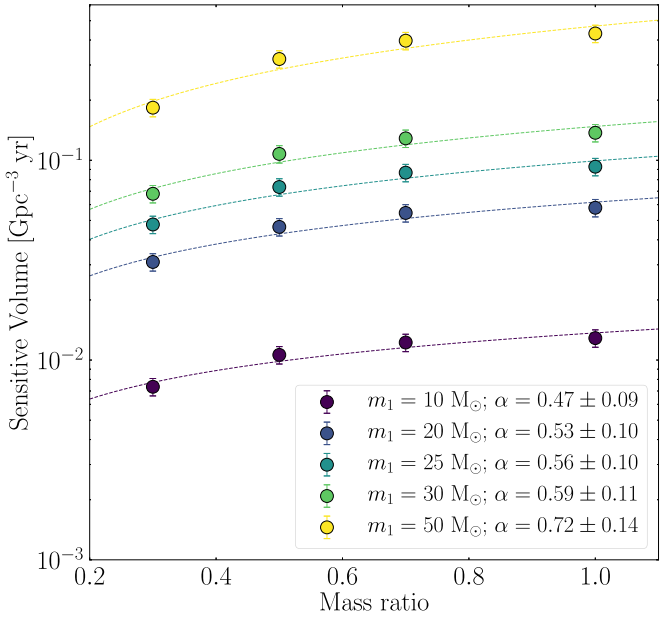

Figure 7. Sensitive redshifted spacetime volume, *VT*, of the LIGO detectors in observation runs O1 and O2 as a function of the mass ratio and for different values of the primary mass. The dotted lines represent least-squares fits of the data. The data points are extracted from Fishbach & Holz (2017).

slope in the range $\beta = 0.47$–0.72. Given the mass of the primary in GW190814, we adopt $\beta = 0.5$ in the main analysis, although we test also the cases $\beta = 0.4$ and $\beta = 0.6$ for the sake of comparison. Table 5 lists the probability $P_{\rm LVC}$ of finding a GW190814-like merger in our database once this "volume weighting" procedure is taken into account. We find that varying the slope in the *VT*–*q* relation causes a maximum variation in $P_{\rm LVC}$ of up to $\lesssim$10%. Due to this, in our calculations we assume a $P_{\rm LVC} = 22\% \pm 2\%$ for solar-metallicity systems and $P_{\rm LVC} = 4.3\% \pm 0.4\%$ for mergers with metal-poor progenitors.

Appendix E
Comparison with Similar Works

In this section we compare our inferred merger rate with recent results obtained through full *N*-body simulations of YCs (Fragione & Banerjee 2020; Rastello et al. 2020).

To perform the comparison, we make use of Equation (3) to derive the mass, half-mass radius, or velocity dispersion of host clusters. For the sake of comparison, Figure 8 shows the link between these three parameters and highlights typical values for Galactic GCs, YCs, and the NC.

Rastello et al. (2020) predict a global merger rate of 28 yr^{-1} Gpc^{-3}, but only ∼36%–55% of these mergers form dynamically, thus implying a *dynamical* merger rate of $\Gamma \simeq 14$ yr^{-1} Gpc^{-3}. The simulations presented by Rastello et al. (2020) focus on star clusters with masses in the range $M = (0.3$–$1) \times 10^3\ M_\odot$ and half-mass radii $R_h = 0.21$–0.25 pc, corresponding to a velocity dispersion $\sigma = 0.67$–1.1 km s^{-1}, according to our Equation (3).

In this range of σ values, our inferred individual merger rate is roughly $\Gamma_{\rm ind} \sim 3 \times 10^{-4}$–$3 \times 10^{-2}$ Gyr^{-1}, depending on the metallicity (the larger the metallicity, the lower the rate) and configuration (BHSTNS produces more mergers).

If we assume that the Rastello et al. (2020) models represent the "normal" population of YCs in an MW-sized galaxy, we

Table 5
GW190814-like Binary Merger Rate Weighted with the Volume–Mass Ratio Observational Bias

Z	$P_{\rm LVC}$		
	$\beta = 0.4$	$\beta = 0.5$	$\beta = 0.6$
0.0002	4.04	4.32	4.63
0.02	23.2	21.8	22.1

Note. Column (1): metallicity. Columns (2)–(4): percentage of models with GW190814-like mass and mass ratio assuming that the accessible volume scales with the mass ratio as q^β.

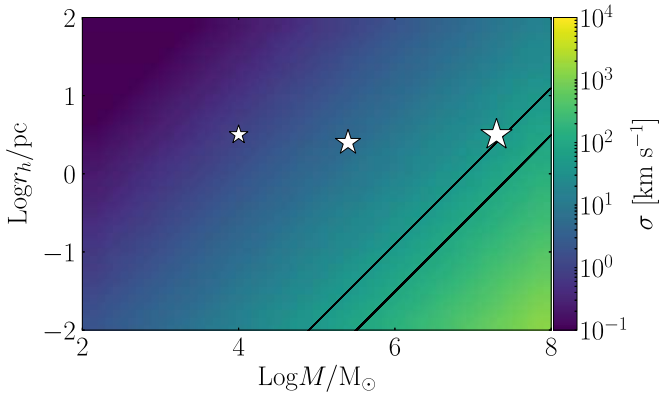

Figure 8. Surface map showing the cluster velocity dispersion as a function of mass and half-mass radius. From left to right, black lines identify clusters with a velocity dispersion of 0.3, 2, 5, 10, 50, and 100 km s^{-1}, respectively. The three black stars identify the typical values for Galactic YCs (Portegies Zwart et al. 2010), GCs (Harris 2010), and the Galactic NC (Feldmeier et al. 2014).

infer a merger rate of $\Gamma_{\rm YC} \sim 0.3$–35 yr^{-1} Gpc^{-3} (see Equation (4) in the main paper), thus bracketing the value inferred from direct models. Note that the assumption that the density of YCs in the local universe is 2.31 Mpc^{-3} (e.g., similar to that of globular clusters; Rodriguez et al. 2016; Fragione & Banerjee 2020; Ye et al. 2020) leads to a merger rate of $\Gamma_{\rm YC} = 7 \times 10^{-4}$–$6.9 \times 10^{-2}$ yr^{-1} Gpc^{-3}. In a more recent work, Fragione & Banerjee (2020) explored the output of 65 *N*-body simulations of clusters with masses $M = 10^4$–$10^5\ M_\odot$ and half-mass radii $R_h = 1$–3 pc (Banerjee 2021). The authors find that 15 NS–BH binaries formed over a 10 Gyr timescale, but none of them merging within a Hubble time. Adopting an average density for the cosmic YC population of $\rho_{\rm YC} \sim 2.31$ Mpc^{-3}, the authors derive an upper limit on the NS–BH merger rate of 3×10^{-3} yr^{-1} Gpc^{-3}. For these models, the velocity dispersion inferred from Equation (2) in the main paper is $\sigma \simeq 1$–5.6 km s^{-1}. According to our calculations, the individual merger rate for these types of clusters is $\Gamma_{\rm ind} = 9.6 \times 10^{-5}$–$0.057$ Gyr^{-1}, depending on the configuration and the metallicity. This implies a local universe merger rate of $\Gamma = \rho\Gamma_{\rm ind} \sim 2.2 \times 10^{-4}$–$0.13$ yr^{-1} Gpc^{-3}, thus embracing predictions for both massive YCs (Fragione & Banerjee 2020) and globular clusters (0.055–5.5 yr^{-1} Gpc^{-3}; Ye et al. 2020).

Despite that our models rely on several physically motivated key assumptions, they capture the essential elements of dynamical NS–BH formation, leading to merger rates in broad agreement with the results obtained with more detailed models. Our models thus provide a complementary view on the NS–BH merger formation process, enabling the possibility to collect a statistically significant sample of candidates that can be used to

place constraints on the properties of the overall NS–BH merger population.

ORCID iDs

Manuel Arca Sedda https://orcid.org/0000-0002-3987-0519

References

Abadie, J., Abbott, B. P., Abbott, R. & LIGO Scientific Collaboration, & Virgo Collaboration 2010, CQGra, 27, 173001
Arca Sedda, M. 2020, CmPhy, 3, 43
Arca Sedda, M., Askar, A., & Giersz, M. 2018, MNRAS, 479, 4652
Arca Sedda, M., & Benacquista, M. 2019, MNRAS, 482, 2991
Arca Sedda, M., Mapelli, M., Spera, M., Benacquista, M., & Giacobbo, N. 2020, ApJ, 894, 133
Arca-Sedda, M., & Capuzzo-Dolcetta, R. 2019, MNRAS, 483, 152
Askar, A., Szkudlarek, M., Gondek-Rosińska, D., Giersz, M., & Bulik, T. 2017, MNRAS Letters, 464, L36
Bahcall, J. N., Hut, P., & Tremaine, S. 1985, ApJ, 290, 15
Bailyn, C. D., Jain, R. K., Coppi, P., & Orosz, J. A. 1998, ApJ, 499, 367
Banerjee, S. 2021, MNRAS, 500, 3002
Belczynski, K., Kalogera, V., & Bulik, T. 2002, ApJ, 572, 407
Binney, J., & Tremaine, S. 2008, Galactic Dynamics (2nd ed.; Princeton, NJ: Princeton Univ. Press)
Breen, P. G., & Heggie, D. C. 2013, MNRAS, 432, 2779
Burrows, A., Radice, D., & Vartanyan, D. 2019, MNRAS, 485, 3153
Clausen, D., Sigurdsson, S., & Chernoff, D. F. 2013, MNRAS, 428, 3618
Dominik, M., Belczynski, K., Fryer, C., et al. 2012, ApJ, 759, 52
Eldridge, J. J., Stanway, E. R., Xiao, L., et al. 2017, PASA, 34, e058
Feldmeier, A., Neumayer, N., Seth, A., et al. 2014, A&A, 570, A2
Fishbach, M., & Holz, D. E. 2017, ApJL, 851, L25
Fragione, G., & Banerjee, S. 2020, ApJL, 901, L16
Freire, P. C. C., Ransom, S. M., Bégin, S., et al. 2008, ApJ, 675, 670
Fryer, C. L., Belczynski, K., Wiktorowicz, G., et al. 2012, ApJ, 749, 91
Georgiev, I. Y., & Böker, T. 2014, MNRAS, 441, 3570
Georgiev, I. Y., Böker, T., Leigh, N., Lützgendorf, N., & Neumayer, N. 2016, MNRAS, 457, 2122
Giacobbo, N., & Mapelli, M. 2018, MNRAS, 480, 2011
Giesers, B., Dreizler, S., Husser, T.-O., et al. 2018, MNRAS, 475, L15
Goodman, J., & Hut, P. 1993, ApJ, 403, 271
Harris, W. E. 2010, arXiv:1012.3224
Heggie, D., & Hut, P. 2003, CQGra, 20, 4504
Heggie, D. C. 1975, MNRAS, 173, 729
Hurley, J. R., Tout, C. A., & Pols, O. R. 2002, MNRAS, 329, 897
Jackson, R. J., Jeffries, R. D., Wright, N. J., et al. 2020, MNRAS, 496, 4701
Kremer, K., Ye, C. S., Rui, N. Z., et al. 2020, ApJS, 247, 48
Kuhn, M. A., Hillenbrand, L. A., Sills, A., Feigelson, E. D., & Getman, K. V. 2019, ApJ, 870, 32
Liu, B., & Lai, D. 2021, MNRAS, 502, 2049
Lu, W., Beniamini, P., & Bonnerot, C. 2021, MNRAS, 500, 1817
Mapelli, M., Spera, M., Montanari, E., et al. 2020, ApJ, 888, 76
Marchant, P., Langer, N., Podsiadlowski, P., et al. 2017, A&A, 604, A55
McKernan, B., Ford, K. E. S., & O'Shaughnessy, R. 2020, MNRAS, 498, 4088
Mikkola, S., & Merritt, D. 2008, AJ, 135, 2398
Mikkola, S., & Tanikawa, K. 1999, MNRAS, 310, 745
Morscher, M., Pattabiraman, B., Rodriguez, C., Rasio, F. A., & Umbreit, S. 2015, ApJ, 800, 9
Özel, F., Psaltis, D., Narayan, R., & Santos Villarreal, A. 2012, ApJ, 757, 55
Peters, P. C. 1964, PhRv, 136, B1224
Piskunov, A. E., Kharchenko, N. V., Röser, S., Schilbach, E., & Scholz, R. D. 2006, A&A, 445, 545
Piskunov, A. E., Schilbach, E., Kharchenko, N. V., Röser, S., & Scholz, R. D. 2007, A&A, 468, 151
Podsiadlowski, P., Langer, N., Poelarends, A. J. T., et al. 2004, ApJ, 612, 1044
Portegies Zwart, S. F., McMillan, S. L. W., & Gieles, M. 2010, ARA&A, 48, 431
Rastello, S., Mapelli, M., Di Carlo, U. N., et al. 2020, MNRAS, 497, 1563
Rodriguez, C. L., Amaro-Seoane, P., Chatterjee, S., et al. 2018, PhRvD, 98, 123005
Rodriguez, C. L., Chatterjee, S., & Rasio, F. A. 2016, PhRvD, 93, 084029
Safarzadeh, M., & Loeb, A. 2020, ApJL, 899, L15
Sigurdsson, S., & Phinney, E. S. 1993, ApJ, 415, 631
Soubiran, C., Cantat-Gaudin, T., Romero-Gómez, M., et al. 2018, A&A, 619, A155
Spera, M., & Mapelli, M. 2017, MNRAS, 470, 4739
Spera, M., Mapelli, M., Giacobbo, N., et al. 2019, MNRAS, 485, 889
The LIGO Scientific Collaboration, & the Virgo Collaboration et al. 2020, ApJL, 896, L44
Thompson, T. A., Kochanek, C. S., Stanek, K. Z., et al. 2019, Sci, 366, 637
Tsokaros, A., Ruiz, M., & Shapiro, S. L. 2020, ApJ, 905, 48
Wyrzykowski, Ł., & Mandel, I. 2020, A&A, 636, A20
Yang, Y., Bartos, I., Haiman, Z., et al. 2019, ApJ, 876, 122
Yang, Y., Gayathri, V., Bartos, I., et al. 2020, ApJL, 901, L34
Ye, C. S., Fong, W.-f., Kremer, K., et al. 2020, ApJL, 888, L10
Zevin, M., Spera, M., Berry, C. P. L., & Kalogera, V. 2020, ApJL, 899, L1
Ziosi, B. M., Mapelli, M., Branchesi, M., & Tormen, G. 2014, MNRAS, 441, 3703